

Dynamic Domains in Strongly Driven Ferromagnetic Films

K. Mayes, T. Plefka,* and H. Sauer mann

Theoretische Festkörperphysik, Technische Universität Darmstadt, D-64289 Darmstadt, Germany

(Dated: January 21, 2022)

The spatiotemporal structure formation problem is investigated in the region far above the transverse ferromagnetic resonance instability. The investigations are based on the dissipative Landau-Lifshitz equation and have been performed on a model which takes external fields, isotropic exchange fields, anisotropy fields and the demagnetizing part of the dipolar field into consideration. The numerical simulations for these models exhibit stationary domain structure in the rotating frame. Employing analytical methods and simplifying the model, certain features, such as the magnetization within the domains and the proportion of the system in each domain, are described analytically.

PACS numbers: 76.50+g, 75.60.Ch

I. INTRODUCTION

Ferromagnetic systems driven by external magnetic fields have been under investigation for many years [1]. Early work by Suhl already showed that there is a threshold of the pump amplitude where the uniform state becomes unstable to homogeneous driving fields [2]. When the difference between the pump field and its critical value is small (the weakly nonlinear case), the experimental findings can be analyzed by extensions of the theory of Suhl as reviewed in [3]. The pattern formation in such a system can be described by amplitude equations [4, 5].

However, when the probe is *strongly* driven, such perturbative procedures break down. One-dimensional numerical simulations have predicted dynamic domains for a model including a transversely rotating field [6]. Dynamic domains are stable solutions to the equations of motion. In the reference frame rotating with the driving field they exhibit a stationary domain structure, like that known from static domains, yet in the lab frame their position is stationary while the magnetization within the domains rotates at different angles. Plefka also obtained dynamic domains in one dimension by numerical simulation and was able to explain characteristic elements of the structure analytically [7] for a very simplified model.

The experimental difficulties involved with large pump amplitudes were solved already twenty years ago [8]. Renewed interest in this topic has led to recent work, where, using the Faraday effect, dynamic domains were observed in garnet films driven by high power inhomogeneous driving fields [9].

The length scales of the patterns we are interested in are large compared to the atomic distance of such substances and so the relevant quantity is a macroscopic variable, the local magnetization $\mathbf{m}(\mathbf{r}, t)$. Using a model that includes a saturating static field and a strong transverse pump field [12], we consider the structures occur-

ring in a ferromagnetic film of side L with normal in the z -direction.

The paper is organized as following: In Sec.II the physical model is described which enters in the Landau-Lifshitz Equation via the effective fields. The numerical results for the various dynamical domains are presented in Sec. III. Employing simplifications of the original model the linear stability of the structures found is considered in Sec. IV leading to partial description of the numerical results. Conclusions are presented in Sec.V.

II. LANDAU-LIFSHITZ EQUATION

The dynamics of $\mathbf{m}(\mathbf{r}, t)$ are described by the Landau-Lifshitz equation [10, 11]:

$$\partial_t \mathbf{m} = -\mathbf{m} \times \mathbf{h}_{\text{eff}} - \Gamma \mathbf{m} \times (\mathbf{m} \times \mathbf{h}_{\text{eff}}) \quad (1)$$

Γ is a dimensionless damping coefficient. The effective magnetic field \mathbf{h}_{eff} is made up of both external and internal magnetic fields:

$$\begin{aligned} \mathbf{h}_{\text{eff}} = & H \mathbf{e}_z + h (\cos(\omega t) \mathbf{e}_x + \sin(\omega t) \mathbf{e}_y) \\ & + J \nabla^2 \mathbf{m} - \overline{m}_z \mathbf{e}_z + K m_z \mathbf{e}_z \end{aligned} \quad (2)$$

These terms are, in order of appearance: a static field of magnitude H in the z -direction (perpendicular to the plane of the film); an in-plane pump field with amplitude h and frequency ω ; an isotropic exchange field ($J > 0$); the demagnetizing part of the dipolar field, describing the geometry of the film; and a uniaxial anisotropy, also in the z -direction.

The explicit time dependence of (1) is removed by a transformation to the rotating reference frame, yielding

$$\partial_t \mathbf{m} = -\mathbf{m} \times (\mathbf{h}_{\text{eff}} - \omega \mathbf{e}_z) - \Gamma \mathbf{m} \times (\mathbf{m} \times \mathbf{h}_{\text{eff}}) \quad (3)$$

while the effective magnetic field now has the form

$$\mathbf{h}_{\text{eff}} = H \mathbf{e}_z + h \mathbf{e}_x + J \nabla^2 \mathbf{m} - \overline{m}_z \mathbf{e}_z + K m_z \mathbf{e}_z \quad (4)$$

*Electronic address: timm@arnold.fkp.physik.tu-darmstadt.de

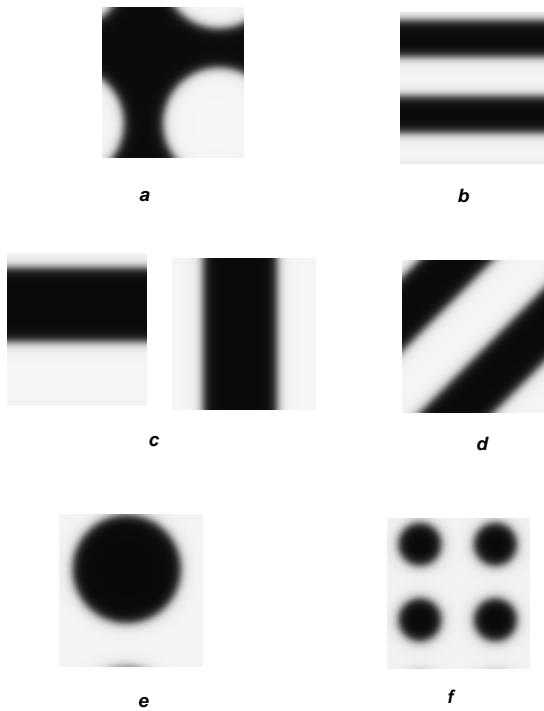


FIG. 1: Dynamically stable domain states obtained at the same parameter values: $\omega = H = 3$, $h = 2$, $J = 10$, $K = 5$, $\Gamma = 0.1$. a) “spin-up” bubble, period L ; b) horizontal stripes, period $L/2$; c) horizontal and vertical stripes, period L ; d) diagonal stripes, period $\sqrt{L/2}$; e) “spin-down” bubble, period L ; f) “spin-down” bubble, period $L/2$

An alternative, frequently used form of the Landau-Lifshitz equation is the Gilbert form

$$\partial_t \mathbf{m} - \Gamma \mathbf{m} \times \partial_t \mathbf{m} = - (1 + \Gamma^2) \mathbf{m} \times \left[\mathbf{h}_{\text{eff}} - \frac{\omega}{1 + \Gamma^2} \mathbf{e}_z + \frac{\Gamma \omega}{1 + \Gamma^2} \mathbf{m} \times \mathbf{e}_z \right]. \quad (5)$$

This is obtained by multiplying equation (3) from the left by $\Gamma \mathbf{m} \times$ and recalling that $\mathbf{m} \cdot \mathbf{m} = 1$. The damping coefficient Γ is the same in both the Gilbert form of the Landau-Lifshitz equation (5) and the common form (3).

Throughout this work we present results in the rotating reference frame. We recall that static results in this frame of reference transform to structures rotating with frequency ω in the x - y plane in the laboratory frame. Hence a state that is *statically* stable in the rotating reference frame is *dynamically* stable in the lab frame.

III. NUMERICAL SIMULATION

We simulate equation (3) with (4) on a vector-parallel computer and workstations, using a spectral approach to deal with the internal field contributions. The number of mesh points for the two-dimensional system was varied up to 256×256 and it is seen that a minimum spatial grid size of 64×64 is necessary to recognize to

good accuracy all magnetic structures that are also visible with a larger number of mesh points. Periodic boundary conditions are used. For 64×64 mesh points, the boundary conditions also have no effect on the structures within the system. This is confirmed by also performing the simulations with unpinned spins, and observing that the same results are obtained. A Euler integration scheme is sufficient and therefore used for the time integration of the system. Indeed more advanced methods, like Runge-Kutta and NDSolve of Mathematica, give essentially identical numerical results.

Throughout the course of a simulation we require that the magnitude of the magnetization remain constant $|\mathbf{m}| = 1$. However, the accumulation of numerical errors means that this is not the case, and the magnetization tends to drift away from the value one. Therefore we add an additional Bloch-like damping term to the equation of motion (3) that recalls the length of the magnetization vector back to one at each time step. This Bloch damping, although a reaction to a numerical artifact, is also justified physically [11].

To investigate systematically the presence of dynamically stable structures, all numerical and physical parameters except the amplitude of the driving field are kept constant ($H = \omega = 3$, $J = 10$, $K = 5$, $\Gamma = 0.1$), while h is varied from $h = 0$ upwards. Depending on the initial states and on the value of h , different coexisting dynamically stable solutions are found.

A. Homogeneous State

The solution found most frequently in numerical simulations is the homogeneous or uniform solution. In this case, all the spins throughout the system rotate at the same frequency, in phase, and with the same constant m_z . The dynamically stable homogeneous state is found numerically for values of h below a certain critical value $h_{c1} \approx 3.7$ and above another critical value $h_{c2} \approx 4.9$.

B. Stripes and Bubbles

Some of the two-domain dynamically stable structures also found are shown in Figure 1. This is a shaded contour plot of the m_z component of the magnetization throughout the system. The dark areas depicted are those where $m_z < 0$ while the light areas imply $m_z > 0$. Figure 1 makes no statement about the x and y components of the magnetization, which (apart from at the wall) are spatially homogeneous and vary periodically in time with period ω . This implies that the spins within the domains rotate in the x - y plane in phase and at the same frequency.

The simulations were performed with a great many different initial conditions. The results shown in Figure 1 are characteristic of *all* the dynamic domain results obtained, i.e. dynamically stable domain states either have

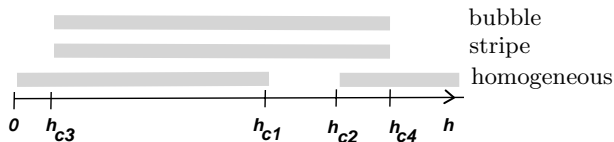


FIG. 2: Schematic view of where the homogeneous, stripe and bubble solutions are found numerically, h is the amplitude of the driving field

either translational symmetry (**b**, **c** and **d**) or cylindrical symmetry (**a**, **e** and **f**) in the z -component of the magnetization.

It is observed that dynamically stable domain states only exist between two values of the driving field, called $h_{c3} \approx 0.2$ and $h_{c4} \approx 5$. As we approach the upper bound h_{c4} the domain states become ever more flattened out, until eventually at h_{c4} the domain state merges into the homogeneous state. This continuous transition is in direct contrast to the lower bound h_{c3} where a well-defined domain state suddenly no longer exists. The values of h_{c3} and h_{c4} are seen to be the same whether bubbles or stripes are under investigation.

C. Wall Structure

The spatially distinct uniform regions are separated by a domain wall. Here the magnetization does not jump from the value in one domain to the next, but rather varies continuously across the finite wall width. The spins inside the wall rotate at the same frequency with the rest of the system, but with a phase shift compared to the spins within the domains. In the domain wall all the spins are parallel. In particular, this is also true for the bubble domain wall and so the whole structure including wall is *not* rotationally symmetric. The rotational symmetry of the system is broken by the presence of the driving field h . Such bubble domains are always obtained, even if rotationally symmetric initial conditions are used.

The structure of the wall differs depending on h . For small h there is a large negative m_y component of the magnetization. As h increases, m_x dominates ever more at the center of the wall. In addition, the width of the wall increases with h . We noted above that the domains themselves become flattened out. This, together with the ever widening wall, means that it is difficult to say precisely when the domain state merges into the homogeneous state at the upper bound h_{c4} .

D. Hysteresis

As indicated in Figure 2, there is tristability in the system, and which pattern actually occurs depends on the initial conditions of the system. Two hysteresis loops occurring in the system are shown in Figure 3. In particular, the behavior of the system at h_{c3} is of interest. We

select as an initial state a domain state which would be stable just above h_{c3} . Reducing h a little below the critical value h_{c3} , the two walls on either side of the “spin-down” domain begin to move towards each other, and the magnetization within the walls to rotate faster and faster than the angular frequency of the driving field. Eventually the walls collide and leave the system in a homogeneous “spin-up” state. This process is shown in Figure 4. The velocity of walls in this transient state is smaller the closer we are to the value $h = h_{c3}$, and it can take up to $60T$, where $T = 2\pi/\omega$ is the period of the driving field, for the wall collision to occur.

IV. ANALYTICAL INVESTIGATION

A. Homogeneous Solution

Homogeneous solutions must satisfy the following conditions

$$\nabla^2 \mathbf{m} = 0 \quad , \quad \overline{m}_z = m_z \quad .$$

and so the effective magnetic field becomes:

$$\mathbf{h}_{\text{eff}} = H\mathbf{e}_z + h\mathbf{e}_x + (K-1)m_z\mathbf{e}_z \quad . \quad (6)$$

We insert (6) into equation (5) and note that for steady state solutions ($\partial_t \mathbf{m} = 0$) the expression in square brackets in (5) must be parallel to \mathbf{m} , with some unknown proportionality factor μ :

$$h\mathbf{e}_x + (\delta + (K-1)m_z)\mathbf{e}_z + \gamma\mathbf{m} \times \mathbf{e}_z = \mu\mathbf{m} \quad , \quad (7)$$

where we have introduced the following definitions:

$$\delta = H - \frac{\omega}{1 + \Gamma^2} \quad , \quad \gamma = \frac{\Gamma\omega}{1 + \Gamma^2} \quad . \quad (8)$$

The parameter δ is a measure of the deviation of the system from resonance and is called the detuning, while γ is the rescaled frequency.

Taking the scalar product of equation (7) with \mathbf{e}_x , \mathbf{e}_y and \mathbf{e}_z respectively and eliminating the unknown factor μ yields two equations for the 3 components of \mathbf{m} . A third equation is obtained from the requirement that $|\mathbf{m}| = 1$. We obtain a fourth order polynomial in m_z :

$$\begin{aligned} & [(K-1)^2 + \gamma^2] m_z^4 + 2\delta(K-1)m_z^3 + [h^2 + \delta^2 \\ & - (K-1)^2 - \gamma^2] m_z^2 - 2\delta(K-1)m_z - \delta^2 = 0 \end{aligned} \quad (9)$$

Either 2 or 4 solutions to equation (9) are found, depending on the parameter regime. A saddle-node bifurcation separates the region of two solutions from that with four solutions.

The stability of these four fixpoint solutions is discussed by means of a linear stability analysis (see Appendix). Figure 5 shows the components of the magnetization for that fixpoint where $m_z > 0$, and the positions of h_{c1} and h_{c2} , between which this fixpoint is unstable to nonuniform perturbations with wavenumber $k \rightarrow 0$. For comparison, the dynamically stable homogeneous states found numerically are also shown.

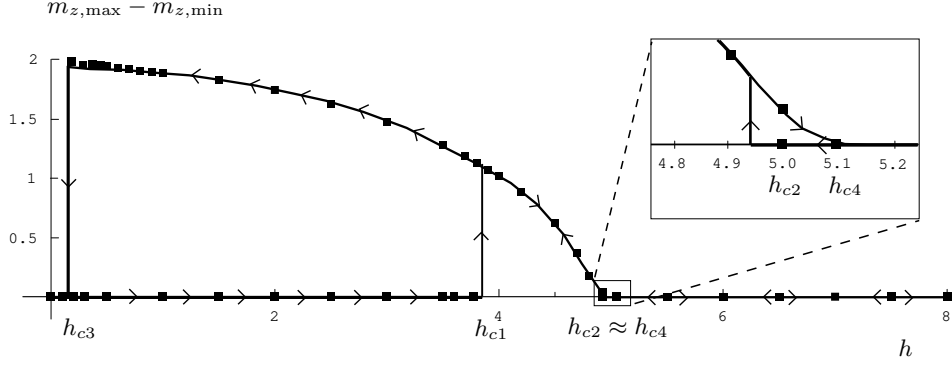


FIG. 3: Hysteresis between the homogeneous and domain solutions. The figure plots $m_{z,\max} - m_{z,\min}$ vs h , the amplitude of the driving field. For the homogeneous state $m_{z,\max} - m_{z,\min} = 0$, while for bubble and stripe domains $m_{z,\max} - m_{z,\min} > 0$. Each dot is the result of a numerical simulation. Arrows indicate the direction of change of the driving field h and the direction of transition. There is a sharp transition from the uniform state to domains at $h_{c1} \approx 3.7$ and from the domain state to the homogeneous state at $h_{c3} \approx 0.2$. The region around $h \approx 5$ is enlarged to show more clearly the sharp transition from the homogeneous state to the domain state at $h_{c2} \approx 4.9$ and the continuous transition from the domain state to the homogeneous state at the somewhat higher value of h_{c4} .

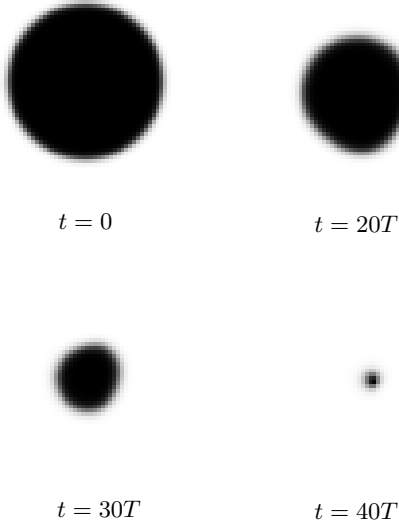


FIG. 4: Disintegration of a spin-up bubble in time for a driving field amplitude just below the critical amplitude h_{c3}

B. Domain Solution

We make a simple ansatz to describe the magnetization in a two-domain state:

$$\mathbf{m}(\xi) = \begin{cases} \mathbf{m}^{(1)} & 0 < \xi < Lq \\ \mathbf{m}^{(2)} & Lq < \xi < L(1-q) \end{cases} \quad (10)$$

i.e. we consider only the magnetization within each domain $i = 1, 2$, and imagine ourselves to be a considerable distance away from the domain walls. The quantity q describes the proportion of the system in each domain.

Again we look for steady state solutions ($\partial_t \mathbf{m}^{(i)} = 0$), and demand that the spatial inhomogeneity in each domain vanish ($\nabla^2 \mathbf{m}^{(i)} = 0$). The demand that the term

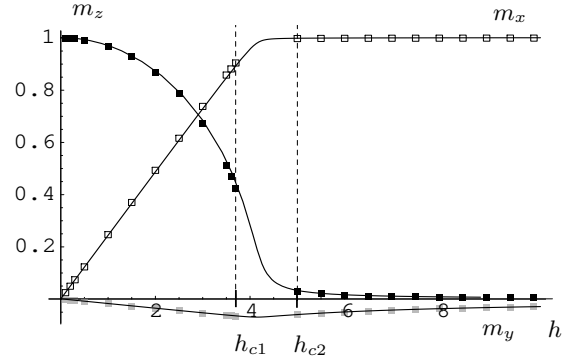


FIG. 5: Dynamically stable homogeneous states at the parameter values: $H = \omega = 3$, $J = 10$, $K = 5$ for different values of h . The solid lines show the m_x , m_y and m_z components of the magnetization determined analytically from Eq. (9), while the dots represent results from numerical simulation. The critical values $h_{c1} = 3.7$ and $h_{c2} = 4.9$ as shown are both determined analytically from Eq. (A7) and observed in numerical simulations

in square brackets in (5) be parallel to \mathbf{m} yields:

$$-\mathbf{h}_{\text{eff}}^{(i)} + \frac{\omega}{1 + \Gamma^2} \mathbf{e}_z - \frac{\Gamma\omega}{1 + \Gamma^2} \mathbf{m}^{(i)} \times \mathbf{e}_z = \mu^{(i)} \mathbf{m}^{(i)} \quad (11)$$

with

$$\mathbf{h}_{\text{eff}}^{(i)} = H \mathbf{e}_z + h \mathbf{e}_x - \overline{m}_z \mathbf{e}_z + K m_z^{(i)} \mathbf{e}_z \quad (12)$$

These two equations for $\mathbf{m}^{(1)}$ and $\mathbf{m}^{(2)}$ are not independent, but rather are coupled via the demagnetizing term \overline{m}_z which holds for the entire system and appears in each effective field $\mathbf{h}_{\text{eff}}^{(i)}$. Using the ansatz (10) we write down the demagnetizing term as

$$\overline{m}_z = \frac{1}{L} \int_0^L m_z(\xi) d\xi = q m_z^{(1)} + (1-q) m_z^{(2)} \quad (13)$$

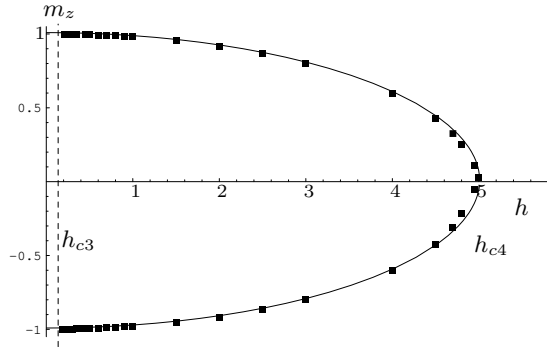


FIG. 6: The z -component of the magnetization within dynamic domains as obtained from numerical simulations and analytical calculation for different values of h . Each pair of dots for a given value of h corresponds to the m_z values far from the domain wall for a single numerically stable simulation; the solid lines show the analytical result Eq. (18). The upper bound $h_{c4} = 5.0037$ is both calculated from Eq. (20) and observed numerically, while the lower bound $h_{c3} = 0.2$ is only observed numerically

A further ansatz still needs to be made to obtain domain solutions, and motivated by the symmetry of the numerical results we set:

$$\begin{aligned} m_x^{(1)} &= m_x^{(2)} =: m_x, \\ m_y^{(1)} &= m_y^{(2)} =: m_y, \\ m_z^{(1)} &= -m_z^{(2)}. \end{aligned} \quad (14)$$

Although this symmetry is not inherent in the equations of motion, it is observed in all numerical simulations without exception and, more importantly, it fixes q and permits a simple closed solution form.

By taking the scalar product of (11) for $i = 1, 2$ with \mathbf{e}_x , \mathbf{e}_y and \mathbf{e}_z and eliminating the unknown $\mu^{(i)}$, we find consistency only if

$$\overline{m}_z = \delta. \quad (15)$$

This is an equilibrium condition for dynamic domains that fixes the proportion of the system in each domain. The effective magnetic field (12) in each domain i is now

$$\mathbf{h}_{\text{eff}}^{(i)} = (H - \delta)\mathbf{e}_z + h\mathbf{e}_x + Km_z^{(i)}\mathbf{e}_z. \quad (16)$$

Comparing equation (16) with (6), we see that all results from the homogeneous calculation in Section IV A can now be applied, providing H is replaced by $H - \delta$ (thus δ is replaced by $(H - \delta) - \frac{\omega}{1+\Gamma^2} = 0$) and K by $K + 1$. Equation (9) then becomes

$$m_z^{(i)4}(K^2 + \gamma^2) + m_z^{(i)2}(h^2 - K^2 - \gamma^2) = 0 \quad (17)$$

with solutions

$$m_z^{(i)} = \pm \sqrt{1 - \frac{h^2}{K^2 + \gamma^2}}. \quad (18)$$

The other components of the magnetization are also simply expressed as

$$m_x = \frac{hK}{K^2 + \gamma^2}, \quad m_y = -\frac{\gamma h}{K^2 + \gamma^2}. \quad (19)$$

Figure 6 shows the z -component of the magnetization within each domain, as given in (18) and compared to numerical simulations. We note that the domain solution can only exist for

$$h < \sqrt{K^2 + \gamma^2}. \quad (20)$$

A linear stability analysis (see Appendix) shows that the simple domain state (10) is stable for *all* values of h where the solution exists. This is in contrast to the numerical evidence, which indicates that there is a lower bound (shown as $h = h_{c3} = 0.2$ in Figure 6) below which no numerical domain solutions exist. There is *no* indication of such a lower bound in any calculations carried out using the ansatz (10).

We recall that the ansatz (10) does *not* describe an entire dynamic domain, only that part far from the domain wall. Therefore any criteria for stability determined in performing a linear stability analysis on (10) will be only *necessary* conditions for stability, and not *sufficient* conditions. Critically, we have neglected any description of the shape or dynamics of the domain wall, and merely assumed a discontinuous transition from one domain to the next. In order to obtain a full description of dynamic domains, and, in particular, to determine the position of the lower bound h_{c3} , it will be necessary to include the wall and consider its effect on the stability of the system.

V. CONCLUSIONS

This work presents a model for a ferromagnetic film in which the exchange, dipolar and anisotropy effects are taken into account. Numerical simulation shows, depending on the amplitude of the transverse pump field applied, different coexisting homogeneous states and dynamic domain structures. The homogeneous state and its stability is wholly understood, and, using a simple model, certain features of the dynamic domain state are also clarified. The magnetization within the domains is determined, as is the proportion of the system in each dynamic domain. Nevertheless a lower bound for the existence of dynamic domains is observed in the numerical simulations that is not found with the simple domain-state model.

An extension to this work has to include the effect of the domain wall, both its structure and its dynamics. Such an extension has been worked out [12] and will be published separately [13] leading to an understanding of the numerical results in their entirety.

Acknowledgments

We wish to acknowledge interesting discussions with H. Dötsch and T. Wöbbeking

APPENDIX A: LINEAR STABILITY ANALYSES

1. Homogeneous Solution

We denote the basic solution computed above as \mathbf{m}_0 . We then add a small time and space dependent perturbation to \mathbf{m}_0 , in particular we consider one Fourier mode of such a perturbation:

$$\mathbf{m}(\xi, t) = \mathbf{m}_0 + \delta\mathbf{m}(\xi, t) = \mathbf{m}_0 + \varepsilon\mathbf{m}_1(t)e^{ik\xi} \quad . \quad (\text{A1})$$

Now the magnetization $\mathbf{m}(\xi, t)$ must have magnitude 1. Thus \mathbf{m}_1 must lie in a plane perpendicular to \mathbf{m}_0 :

$$\mathbf{m}_0 \cdot \mathbf{m}_1 = 0 \quad . \quad (\text{A2})$$

We insert ansatz (A1) into the Landau-Lifshitz equation in the rotating reference frame (3) and sort for powers of ε . To order ε :

$$\begin{aligned} -\dot{\mathbf{m}}_1 &= \mathbf{m}_1 \times (\mathbf{h}_{\text{eff},0} - \omega\mathbf{e}_z) + \mathbf{m}_0 \times \mathbf{h}_{\text{eff},1} + \\ &\Gamma [\mathbf{m}_1 \times (\mathbf{m}_0 \times \mathbf{h}_{\text{eff},0}) + \mathbf{m}_0 \times (\mathbf{m}_1 \times \mathbf{h}_{\text{eff},0}) + \\ &\quad \mathbf{m}_0 \times (\mathbf{m}_0 \times \mathbf{h}_{\text{eff},1})] \quad , \end{aligned} \quad (\text{A3})$$

where we have introduced

$$\begin{aligned} \mathbf{h}_{\text{eff},0} &= H\mathbf{e}_z + h\mathbf{e}_x + (K-1)m_{z,0}\mathbf{e}_z \quad , \\ \mathbf{h}_{\text{eff},1} &= -Jk^2\mathbf{m}_1e^{ik\xi} + Km_{z,1}\mathbf{e}_ze^{ik\xi} - \overline{\delta m_z}\mathbf{e}_z \quad . \end{aligned}$$

The field $\mathbf{h}_{\text{eff},1}$ depends on whether the case $k = 0$ or $k \neq 0$ is being considered, i.e. whether the perturbation $\delta\mathbf{m}$ is uniform or non-uniform. If $k = 0$, $\overline{\delta m_z} = m_{z,1}$, whereas if $k \neq 0$, the fluctuations averaged over the entire system are zero and so $\overline{\delta m_z} = 0$. Therefore

$$\begin{aligned} \text{for } k = 0, \quad &\mathbf{h}_{\text{eff},1} = (K-1)m_{z,1}\mathbf{e}_z \quad , \\ \text{for } k \neq 0, \quad &\mathbf{h}_{\text{eff},1} = Km_{z,1}\mathbf{e}_ze^{ik\xi} - Jk^2\mathbf{m}_1e^{ik\xi} \quad . \end{aligned}$$

We introduce a coordinate system defined as

$$\mathbf{e}_1 = \mathbf{m}_0, \mathbf{e}_2 = \mathbf{m}_0 \times \mathbf{e}_z, \mathbf{e}_3 = \mathbf{m}_0 \times (\mathbf{m}_0 \times \mathbf{e}_z) \quad . \quad (\text{A4})$$

In this coordinate system \mathbf{m}_1 is written as

$$\mathbf{m}_1(t) = \beta(t)\mathbf{e}_2 + \gamma(t)\mathbf{e}_3$$

and equation (A3) assumes the form

$$\begin{aligned} -\dot{\beta}\mathbf{e}_2 - \dot{\gamma}\mathbf{e}_3 &= (\mathbf{h}_{\text{eff},0} \cdot \mathbf{m}_0 - \omega m_{z,0})(-\beta\mathbf{e}_3 + \gamma\mathbf{e}_2) + \\ &\Gamma(\mathbf{m}_0 \cdot \mathbf{h}_{\text{eff},0})(\beta\mathbf{e}_2 + \gamma\mathbf{e}_3) + \\ &\mathbf{e}_1 \times [\mathbf{h}_{\text{eff},1} + \Gamma\mathbf{e}_1 \times \mathbf{h}_{\text{eff},1}] \quad . \end{aligned} \quad (\text{A5})$$

We examine the four fixpoint solutions of (9) for stability with respect to uniform ($k = 0$) and nonuniform ($k \neq 0$)

perturbations by considering the eigenvalues of the linear operator \underline{L} defined by the right-hand side of equation (A5).

The eigenvalues of the 2×2 matrix \underline{L} for $k = 0$ are positive for two of the four fixpoints. For the other two fixpoints, the trace of \underline{L} for $k \neq 0$ is negative for all values of k , so we only need consider its determinant, given by

$$\text{Det}(L_{k \neq 0}) = (1 + \Gamma^2)(k^4 J^2 + k^2 JP + Q) \quad , \quad (\text{A6})$$

where

$$\begin{aligned} P &= (K(m_{z,0}^2 - 1) + 2\mathbf{m}_0 \cdot \mathbf{h}_{\text{eff},0}) - 2\frac{\gamma}{\Gamma}m_{z,0} \quad , \\ Q &= (\mathbf{m}_0 \cdot \mathbf{h}_{\text{eff},0})(\mathbf{m}_0 \cdot \mathbf{h}_{\text{eff},0} + K(m_{z,0}^2 - 1)) \\ &\quad + \frac{\gamma}{\Gamma}m_{z,0}(\mathbf{m}_0 \cdot \mathbf{h}_{\text{eff},0} + \omega m_{z,0}) \quad . \end{aligned}$$

Varying h , the determinant first becomes negative (and hence the fixpoint unstable) for $k \rightarrow 0$ at critical values of the driving field called h_{c1} and h_{c2} given by

$$P - \sqrt{P^2 - 4Q} = 0 \quad . \quad (\text{A7})$$

2. Domain Solution

The stability analysis of the domain solution is performed analogously to that of the homogeneous solution in Section A1. A small perturbation is added to the magnetization in each domain $i = 1, 2$. As the Fourier modes in the first domain would couple to all of those in the second domain, we instead perform the calculation in real space, writing

$$\mathbf{m}_1^{(i)}(\xi, t) = \beta(\xi, t)^{(i)}\mathbf{e}_2^{(i)} + \gamma(\xi, t)^{(i)}\mathbf{e}_3^{(i)} \quad .$$

We obtain a system of 2 equations for each $(\beta^{(i)}, \gamma^{(i)})$, equivalent to (A5)

$$\begin{aligned} -\dot{\beta}^{(i)}\mathbf{e}_2^{(i)} - \dot{\gamma}^{(i)}\mathbf{e}_3^{(i)} &= \\ &\left[\mathbf{m}_0^{(i)} \cdot \mathbf{h}_{\text{eff},0}^{(i)} - \omega m_{z,0}^{(i)}\right](\beta^{(i)}\mathbf{e}_3^{(i)} + \gamma^{(i)}\mathbf{e}_2^{(i)}) \\ &+ \Gamma(\mathbf{m}_0^{(i)} \cdot \mathbf{h}_{\text{eff},0}^{(i)})(\beta^{(i)}\mathbf{e}_2^{(i)} + \gamma^{(i)}\mathbf{e}_3^{(i)}) \quad (\text{A8}) \\ &+ \left[K(m_{z,0}^2 - 1)\gamma^{(i)} - (\overline{m_z})_1\right](\mathbf{e}_2^{(i)} + \Gamma\mathbf{e}_3^{(i)}) \\ &+ J\left[\beta^{(i)}(\mathbf{e}_3^{(i)} - \Gamma\mathbf{e}_2^{(i)}) + \gamma^{(i)}(-\mathbf{e}_2^{(i)} - \Gamma\mathbf{e}_3^{(i)})\right] \end{aligned}$$

where $\mathbf{h}_{\text{eff},0}^{(i)}$ is defined in (16).

In the case of *uniform* perturbations, equation (A8) reduces to a system of four coupled ordinary differential equations. Numerically computing the eigenvalues of this 4×4 matrix shows that all eigenvalues are negative for $h < h_{c4} = \sqrt{K^2 + \gamma^2}$ and so the domain state is stable to (local) uniform perturbations.

For *non-uniform* perturbations, we discretize equation (A8) by replacing the spatial derivatives with finite difference expressions. For all values of $h < h_{c4} = \sqrt{K^2 + \gamma^2}$,

the real part of the eigenvalue spectrum is strictly negative for both solutions $m_z^{(i)}$ in (18). Hence the domain state is also stable to (local) non-uniform perturbations.

Finally, we may consider what happens when the *position of the wall is displaced from its equilibrium position* given by (15), i.e., additionally letting $q \rightarrow q_0 + \varepsilon q_1(t)$. Again, we obtain a linearized equation of motion. Integrating this equation over a small section of the containing the wall, and then letting the size of this section go to zero

$$\lim_{\varepsilon \rightarrow 0} \int_{Lq_0 - \varepsilon}^{Lq_0 + \varepsilon} \dots d\xi \quad ,$$

we obtain a single equation for $q_1(t)$:

$$\dot{q}_1 = -K [1 - \Gamma(1 - m_{z,0})] q_1 \quad . \quad (\text{A9})$$

The expression in square brackets in (A9) is strictly positive, and so again the domain solution is stable to displacement of the wall from its equilibrium position.

-
- [1] R.W. Damon, *Ferromagnetic resonance at high power*, in *Magnetism*, Vol.I, Editors G.T. Rado and H. Suhl, (1963) Academic Press, New York, London.
 - [2] H. Suhl, J. Phys. Chem. Solids **1** (1957) 209.
 - [3] P.E. Wigen (Editor) , *Nonlinear phenomena and chaos in magnetic materials* , (1994) World Scientific, Singapore and references therein.
 - [4] F.J. Elmer, Phys. Rev. B **53** (1996) 14323.
 - [5] F. Matthäus and H. Sauermann, Z. Phys. B **99** (1996) 611.
 - [6] F.J. Elmer, J. Phys. (Paris) **49** (1988) C8-1597.
 - [7] T. Plefka, Phys. Rev. Lett. **75** (1995) 144.
 - [8] H.Dötsch, J. Mag. Mag. Materials **4** (1977) 180.
 - [9] T. Wöbbeking, H. Dötsch and A.F.Popkov, J. Phys. D **31**(1998) 2751.
 - [10] L.D. Landau and E.M. Lifshitz, Phys. Z. Sowjet. **8** (1935) 153. [Reprint in: *Collected Papers of L.D. Landau* (1965) D. ter Haar (editor) Pergamonn Press , Oxford]
 - [11] D.A. Garanin, Physica A **172** (1991) 470 ; T. Plefka, Z. Phys. B **90**(1993) 447.
 - [12] K. Mayes, *Dynamic Domains in Strongly Driven Ferromagnetic Films*. (2003) Dissertation TU Darmstadt, Darmstadt, <http://www.elib.tu-darmstadt.de/diss/00302>
 - [13] K. Mayes, T. Plefka and H. Sauermann, in preparation.